Dual Wide-band Microstrip Antenna for Wireless Communication Systems

Patrycja Okołot, Marian Wnuk, and Konrad Szczepankiewicz

Military University of Technology, Warsaw, Poland

https://doi.org/10.26636/jtit.2026.3.2635

Submitted: 28 May 2026, Accepted: 9 Jun. 2026

Abstract — This article presents the design of a compact dual wide-band microstrip antenna. It also describes the simulation of its operation and provides the results of electrical parameter and radiation characteristics measurements. The designed antenna is intended to operate in two ranges. The first covers frequencies from 3.8 to 8 GHz and all the U-NII antenna ranges (U-NII-1, U-NI-2A, U-NII-2B, U-NII-2C, U-NII-3, U-NII-4, U-NII-5, U-NII-6, U-NII-7, U-NII-8) defined in the IEEE-802.11a standard (5.150 to 7.125 GHz). The other covers frequencies from 11.34 to 20.64 GHz and the Ku band (from 11.7 to 12.7 GHz). The performance of the antenna, developed using CST Microwave Studio and Matlab software, was verified through simulation. Then, a prototype was manufactured and was subjected to measurements in an anechoic chamber. Results of the simulation and the measurement campaign were compared against six other dual-band antenna designs available in the literature. Comparison of the parameters of the proposed design and characteristics of other antennas with a similar profile, selected from the literature, shows that the operating bandwidth of the proposed solution with respect to the S_{11} parameter is the largest, reaching 88.13% for the lower operating band and 59.93% for the upper operating band.

Keywords — dual band, FDTD method, microstrip antenna, wide band

1. Introduction

In the modern technology landscape, where communication is no longer an option and has long become a key functionality of devices, antennas – including those of the microstrip variety – play a particularly important role. Their compact size, low weight, and ability to be integrated with other electronic devices make them useful in a wide range of applications, including 5G networks [1], [2].

Decisions regarding the allocation of the 4400 – 4800 MHz, 7125 – 7250 MHz, 7750 – 8400 MHz, and 14.8 – 15.35 GHz bands for terrestrial IMT systems are expected to be made soon. The sub-6 GHz operating frequency band includes the n79 (4400 – 5000 MHz) range. Furthermore, Wi-Fi standards typically cover the 5 GHz band (5150 – 5830 MHz). The latest WLAN communication standard divides the 6 GHz band (5925 – 7125 MHz) into Wi-Fi 6E/7 ranges. Therefore, a dual-band antenna covering both the Sub-6 GHz and Wi-Fi 6E/7 frequency ranges may be a promising solution for future communication devices.

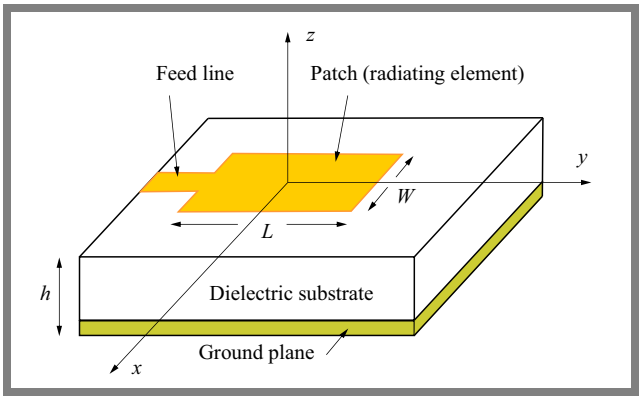


Fig. 1. Microstrip antenna.

Recently, several studies have been published on broadband antennas for 5G sub-6 GHz networks with an operating bandwidth of 11%, e.g. [3]–[8]. To the best of the authors' knowledge, no dual-band antenna designs with a significantly wider operating band have been reported in the literature.

This paper presents a developed model of a dual-band microstrip antenna, implemented in CST Microwave Studio software. The main assumption is that the new solution will be operating in the band covering frequencies from 3.8 to 8 GHz, and a second band covering frequencies from 11.34 to 20.64 GHz, thus fully covering the Ku band (from 11.7 to 12.7 GHz). Another important assumption for the antenna model is its compact size with dimensions no larger than 20 × 25 mm, which is important for its potential application in mobile devices.

2. Design and Modeling of a Dual-band Antenna

Microstrip designs are currently one of the most innovative fields in antenna technology. Microstrip antennas offer numerous interesting features, such as small size, low volume, and flat design making them easy to integrate with end-user applications. Low production costs and high repeatability of specifications, combined with a wide operating frequency range, ensure numerous application opportunities. Low weight allows such antennas to be used on fast flying objects, without exerting any negative impact on their aerodynamic properties.

This work is licensed under a Creative Commons Attribution 4.0 International (CC BY 4.0) License.
For more information, see https://creativecommons.org/licenses/by/4.0/

However, the dielectric substrate used favors the excitation of surface waves which, propagating along the dielectric plane, interfere with the normal operation of the antenna [9]. Other disadvantages of microstrip antennas include a relatively narrow bandwidth and limited power capabilities. This causes mutual coupling, which changes the field distributions on aperture antennas and the current distributions in linear antennas. This phenomenon, in turn, changes the spatial characteristics of antenna radiation and input impedance.

A microstrip antenna consists of a metal radiator (patch) and a ground plane, with both elements separated by a dielectric layer (Fig. 1). The relative permittivity of substrate ε_r varies from 2.2 to 12. Specification of the substrate also controls radiation efficiency, bandwidth, and antenna size. In most cases, microstrip antennas have a rectangular shape, with their crucial parameters determined by patch width W, length L, and thickness of the dielectric layer h characterized by relative dielectric permittivity ε_r [10], [11].

During the modeling process, in the first approximation, the dimensions of the antenna, i.e. length and width, were determined using the transmission line model, defined as follows:

$$L = \frac{c}{2f_r\sqrt{\varepsilon_{re}}} - 2\Delta L\,, \tag{1}$$

$$W = \frac{c}{2f_0\sqrt{\frac{\varepsilon_r+1}{2}}}\,, \tag{2}$$

where ε_{re} is the effective dielectric constant such as:

$$\varepsilon_{re} = \frac{\varepsilon_r+1}{2} + \frac{\varepsilon_r-1}{2}\left(1+12\,\frac{h}{W}\right)^{-1/2}. \tag{3}$$

The width of the radiator determines operating bandwidth and input impedance. An increase in the width of the patch improves radiation efficiency. On the other hand, the antenna's resonant frequency depends on the length of the radiator. After calculations performed in Matlab using Eqs. (1), (2), the width-to-length ratio was determined to be $W/L \approx 1.31$. This value results from Eqs. (1) and (2) for the assumed substrate parameters and operating frequency range.

Radiator extension value ΔL, depending on the effective dielectric constant, laminate height, radiator length and width, is another parameter of the antenna. ΔL is related to the scattering fields occurring at the ends of the radiator. It is determined by the following formula:

$$\Delta L = 0.412\,h\frac{(\varepsilon_{re}+0.300)\,(W/h+0.264)}{(\varepsilon_{re}-0.258)\,(W/h+0.813)}\,. \tag{4}$$

The antenna's input impedance Z, i.e. 50 Ω, depends on the distance from the antenna's edge to the radiator's edge. The value increases as this distance decreases. The radiator's input resistance was then determined as:

$$R_{in} = \frac{1}{G_{10}}\,, \tag{5}$$

where G_{10} is conductance representing radiation, dielectric, and patch/shield losses.

To speed up the calculation of antenna parameters according to Eqs. (1) – (4), a program was created in the Matlab environment, which resulted in determining approximate dimensions of the antenna: W = 13 mm and L = 10 mm.

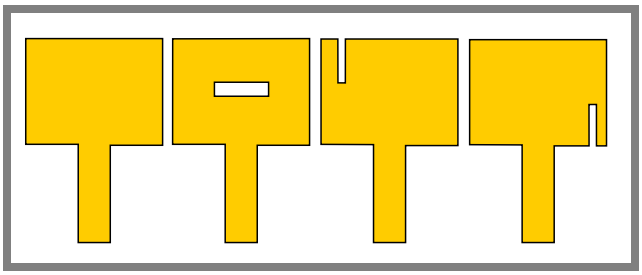


Fig. 2. Steps of iterative antenna design process.

The antenna operates in TM10 and TM01 wave modes [12], [13]. The location of the feed line is determined by the desired wave mode. For TM01 and higher modes, the feed line should be placed on the W side, and if the antenna is to operate in TE10 and higher modes, on the L side. In the case of waves in TM01 and higher modes, the W edges radiate, and in the case of TE10 and higher modes, the L edges radiate. Comparison of both wave modes shows that when the element operates in TM01 and higher wave modes, the quality factor of the system is lower, resulting in a wider operating band.

The method of moments is used most frequently for analyzing microstrip antennas, as it allows to model the current distribution. It is based on the concept of reactions between the base segments and the test functions. The Green function is used for integral equations of the electric field, satisfying the boundary conditions for a metal radiator. Integral equations are discretized into linear equations using the method of moments to obtain a matrix equation [14]. Solving the matrix equations yields the current distribution on the radiator. This distribution, along with the Green function, allows to determine the antenna's radiation pattern in both the near and far fields.

The antenna's substrate may be made of a homogeneous or mixed dielectric ($\varepsilon_r \neq 1$) materials. For a non-homogeneous dielectric, Green's function can only be determined in the spectral domain. For the x axis of the current J_x at the air-dielectric interface and while $z = h$, the electric field components in the spectral domain are [15] as follows.

$$\overrightarrow{E}_x(k_x,k_y,h) = \frac{-j}{\omega\,\varepsilon_0}\left[\frac{k_x^2 k_1 k_2\sin(k_1h)}{\beta^2 TM} + \frac{k_y^2 k_0^2\sin(k_1h)}{\beta^2 TE}\right]J_x\,, \tag{6}$$

$$\overrightarrow{E}_y(k_x,k_y,h) = \frac{-j}{\omega\,\varepsilon_0}\left[\frac{k_x k_y k_1 k_2\sin(k_1h)}{\beta^2 TM} + \frac{k_x k_y k_0^2\sin(k_1h)}{\beta^2 TE}\right]J_x\,, \tag{7}$$

$$\overrightarrow{E}_z(k_x,k_y,h) = \frac{-j}{\omega\,\varepsilon_0}\left(\frac{k_1 k_x\sin(k_1h)}{TM}\right)J_x\,, \tag{8}$$

$$TM = \varepsilon_r k_2\cos(k_1h) + jk_1\sin(k_1h)\,, \tag{9}$$

$$TE = k_1\cos(k_1h) + jk_2\sin(k_1h)\,, \tag{10}$$

$$k_1^2 = k_z^2 = \varepsilon_r k_0^2 - \beta^2 \quad \text{for } 0 < z < h \text{ (layer 1)} \;\; \mathrm{Im}(k_1) < 0\,, \tag{11}$$

$$k_2^2 = k_z^2 = k_0^2 - \beta^2 \quad \text{for } z > h \text{ (layer 2)} \;\; \mathrm{Im}(k_2) < 0\,, \tag{12}$$

$$\beta^2 = k_x^2 + k_y^2\,, \tag{13}$$

where: k_x, k_y, k_1, k_2, k_0, are components of the electromagnetic field, layer 1 is free space and layer 2 is dielectric.

According to [16], [17], a rectangular antenna has a relatively narrow operating bandwidth, not exceeding 10%. A viable way to expand the operating bandwidth is to use a multilayer dielectric structure. However, such solutions complicate the antenna's design and increase its dimensions. Another solution is to introduce slots in the plane of the radiating element. In this case, their dimensions and position are chosen to disrupt the first two modes of the slit's side edge so that their resonant frequencies approach each other, creating a wide operating bandwidth.

Various slot shapes can be found in [18]–[22], including: comb-shaped, double-bend, cross-shaped, U-shaped. The parameters that influence the bandwidth of a microstrip antenna are the slot length and width, as well as its position in the antenna plane. It should be noted that the slot width should be small relative to its length, because the higher resonant mode is sensitive to changes in the horizontal slot length, while the lower resonant mode strongly depends on the slot circumference [23]–[27]. Using Eqs. (6)–(12), both the higher and lower modes, i.e., the slot length and width, were selected to obtain the required antenna bandwidth.

Changes in the slot length and width did not significantly affect the antenna's output impedance. Specific mathematical formulas, even empirical ones, which would determine the exact geometry of the structure and slot position to ensure the antenna achieves a predetermined bandwidth, are not yet available [28], [29].

The tool used to design the microstrip antenna is CST Microwave Studio. This advanced electromagnetic field simulation software allows to design, analyze, and optimize systems and their components in a three-dimensional environment. The program utilizes the finite-difference time-domain (FDTD) method, which allows for accurate broadband simulations. This method is suitable for analyzing both stationary and transient electromagnetic wave behaviors in complex structures. Table 1 summarizes CST output of the designed structure's dimensions and parameters.

The designed antenna has three slots, as shown in Fig. 2. The position and dimensions of these slots were determined through iterative evaluation. The microstrip antenna's radiator is made of 35 µm thick copper, while the dielectric substrate is Rogers FR4 – a material characterized by good electrical properties, a dielectric constant of $\varepsilon_r = 4.3$, a dielectric loss angle of tg $\delta = 10^{-3}$, and a thickness of dielectric layer $b = 1.6$ mm. The antenna is fed by a 3-millimeter microstrip line. This width results from the antenna being designed for standard 50 Ω impedance.

Tab. 1. Simulation parameters used to analyze the proposed system.

Description	Name	Value [mm]
Distance of the top slot from the left edge	W1	1.7
Slot width at the top edge	W2	0.6
Distance of the right edge of the top slot from the right edge	W3	10.7
Distance of the center slot from the left edge	W4	4.0
Length of the center slot	W5	5.0
Distance of the feed line from the left edge	W6	5.0
Width of the feed line	W7	3.0
Distance of the bottom slot from the feed line	W8	3.5
Width of the slot at the bottom edge	W9	0.6
Distance of the left edge of the slot from the right edge	W10	0.9
Ground plane width	W11	20.0
Length of the feed line	L1	9.5
Antenna length	L2	10.0
Length of the top slot	L3	3.9
Distance of the top edge of the center slot from the top edge	L4	4.5
Distance of the bottom edge of the center slot from the bottom edge	L5	4.5
Length of the bottom slot	L6	3.9
Ground plane height	L7	9.0

The basis for selecting the type of slots as well as their dimensions and position was the determination of the s parameter matrix (describing scattering between the device's ports). S_{11} indicates the amount of power reflected from the antenna and is referred to as the reflection coefficient. We assume that the antenna operates correctly for $S_{11} < -10$ dB.

To check the impact of the slots on the antenna's operating bandwidth, a series of simulations was performed using CST. The results for four scenarios: antenna without slots (1), with a horizontal slot (2), with a slot at the top edge (3), and with a slot at the bottom edge (4), are presented in Fig. 2. For each scenario, S_{11} parameters were obtained for the following operating bands (Fig. 3):

1) 16.25 to 20.85 GHz,
2) 3.75 to 8.05 GHz and 10.2 to 21 GHz,

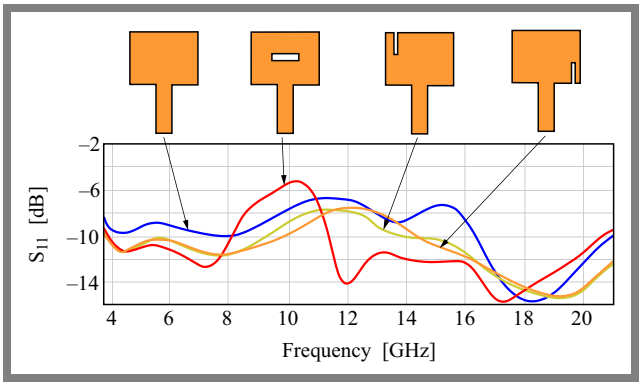


Fig. 3. S_{11} versus frequency for the considered scenarios.

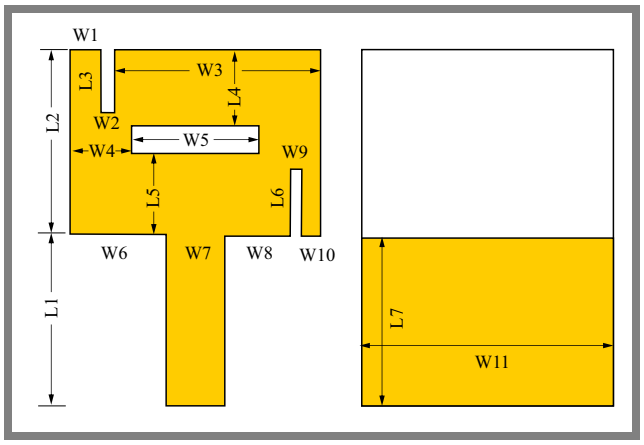


Fig. 4. Front and back side view of optimized antenna.

3) 3.75 to 8.05 GHz and 10.2 to 21 GHz,

4) 3.75 to 8.15 GHz and 11.2 to 21 GHz.

Figure 3 shows that none of the developed cases met the required operating bandwidth. When analyzing the obtained results, one may conclude that the slot located in the lower right corner has the greatest impact on the operating bandwidth. This may be the case as this slot contributes most to the excitation of higher TM modes. Therefore, in the next step, an antenna design including all the slots shown in Fig. 2 to form a comb-like structure was analyzed.

The designed slots allowed for the excitation of higher-order modes according to Eqs. (6)–(13). This iterative design process results from the fact that at this stage, the only method described in the literature for determining the location of slots is the trial-and-error method, which requires extensive design experience. Such an antenna design is presented in Fig. 4, while detailed dimensions of the structure are provided in Tab. 1.

The next step in the analysis was to determine the current distribution. For frequency ranges where the condition $S_{11} < -10$ dB is met, the electric field strength values are roughly similar – see the upper row in Fig. 5. In a scenario where only one frequency band meets the requirements of $S_{11} < -10$ dB, we can conclude that for the selected frequency of 12 GHz, there is a multi-fold increase in the electric field strength value, as shown in bottom row of Fig. 5.

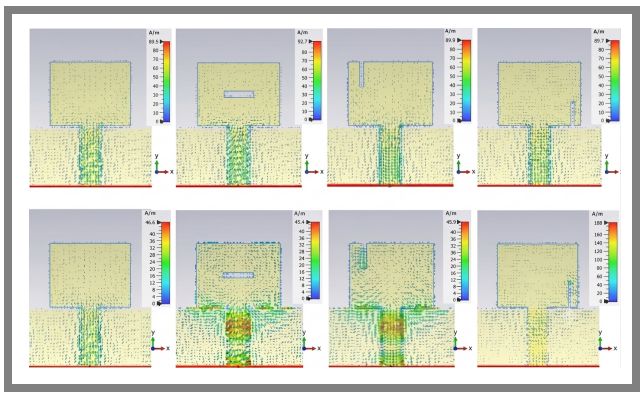


Fig. 5. Current distribution for the frequency of 3.9 GHz (upper row) and 12 GHz (bottom row).

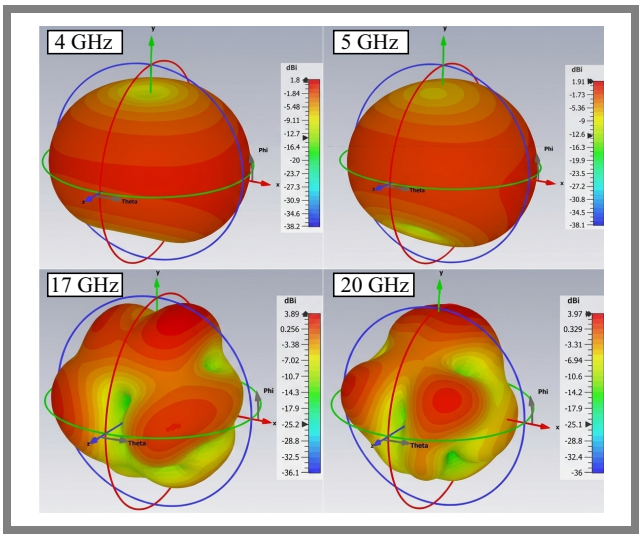


Fig. 6. 3D plot of antenna energy gain.

The radiation pattern describes the spatial distribution of the intensity of the electromagnetic field generated by the antenna. The energy gain, on the other hand, is a measure of the antenna's ability to direct RF energy in each direction. Results of the simulation focusing on the antenna's properties in 3D are presented in Fig. 6.

One may notice there that in the bottom frequency range of 3.9 to 8.11 GHz, the energy gain is significantly lower than in the case of the upper working band of 11.34 to 20.64 GHz. At 4 GHz, the energy gain is 1.8 dBi, and for 20 GHz, it reaches 3.97 dBi. Therefore, it can be concluded that at higher frequencies, the antenna does not provide the expected omnidirectionality.

3. Fabrication and Measurements

To achieve dual-band operation with wide bandwidth, the final antenna utilizes all slots from the design iterations presented in Fig. 2. The final concept was simulated using CST to verify its assumptions and then, after corrections to the shape, size, and radiator size, a prototype of the antenna was manufactured (Fig. 7).

The measurements were conducted under far-field conditions in an anechoic chamber. To eliminate potential interference from the connector, the pins were covered with an RF ab-

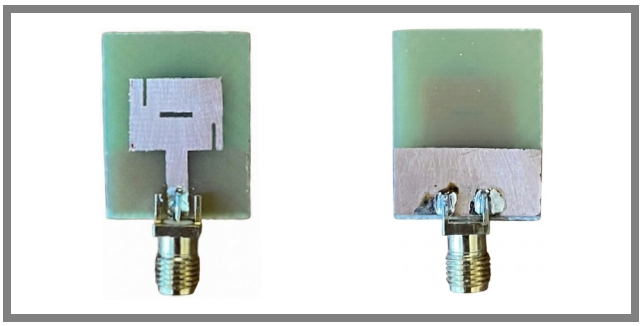


Fig. 7. Fabricated antenna prototype: front and bottom view (right).

Tab. 2. Comparison of packet delivery ratios based on the transmitting node.

Ref.	Footprint area λ_0^2		Profile λ_0		Bandwidth	
[3]	1.1 × 1.1		0.06		25%	
[4]	1.1 × 1.1		0.06		25%	
[5]	0.75 × 0.75		0.045		21.3%	
[6]	0.88 × 0.78		0.11		24.8%	
[7]	1.17 × 0.5		0.039		10%	
[8]	0.58 × 0.39		0.048		14%	
Proposed	Lower band	Upper band	Lower band	Upper band	Lower band	Upper band
	0.396 × 0.496	1.831 × 2.1289	0.0317	0.146	88.13%	59.93%

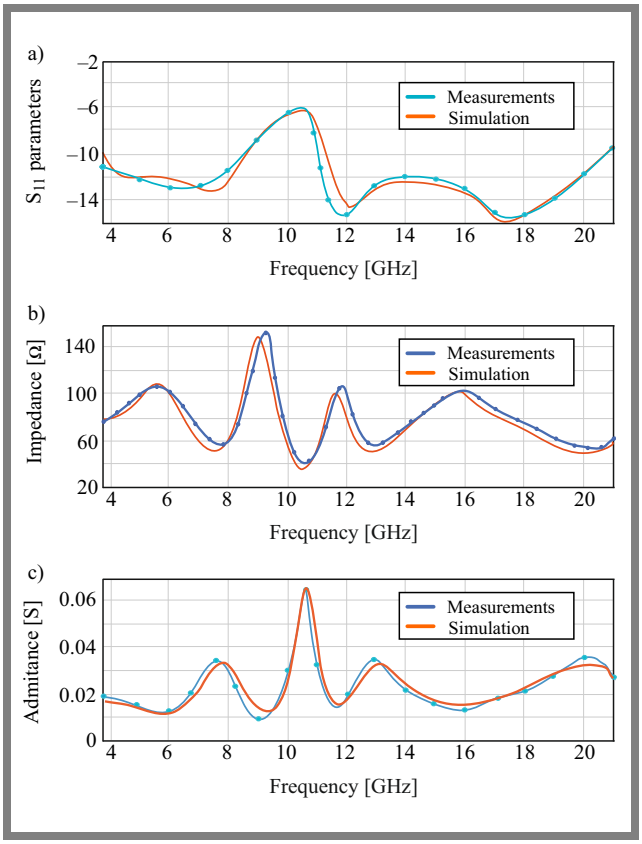


Fig. 8. S_{11} for the proposed antenna a), input impedance b), and admittance c).

sorber. the measurements were performed in accordance with ANSI/IEEE Std 149:1979.

Reflection coefficient S_{11} is defined as the voltage ratio of the reflected wave to the wave that encounters the antenna. A high value of this coefficient indicates that a significant amount of energy is not absorbed by the antenna but is reflected instead, which is unfavorable and can result in lower antenna efficiency. As previously mentioned, for antennas, we assume that the S_{11} parameter should be below –10 dB.

The lowest S_{11} reflection coefficient for the lower band is –12.07 dB at 6.5 GHz and –15.2 dB at 17.23 GHz for the upper band, according to Fig. 8a. Such values indicate good matching of the antenna to the transmission line, minimizing power losses while maintaining acceptable system performance. This matching is crucial to ensuring optimal antenna performance in its operating environment.

The input impedance is a key parameter of any antenna, as it determines the quality of matching with the RF power source, which directly affects performance, bandwidth, and radiation efficiency. As can be seen in Fig. 8b, the input impedance for the lower band at its cutoff frequencies is 57 and 40 Ω, respectively. The expected 50 Ω value was obtained at 6.72 GHz. For the upper frequency band, the input impedance for the cutoff frequencies reached amounts to 62 and 32 Ω. The 50 Ω threshold was obtained for frequencies of 12.14, 14.01, and 17.93 GHz.

The antenna input admittance Y_{11} is the reciprocal of input impedance Z_{11}. This is an important parameter in analyzing any antenna, as it describes how easily current flows into the antenna from an external source. Admittance is a complex quantity and consists of a real part and an imaginary part.

Admittance for a microstrip antenna should approach a conductance value of 0.02 S and a susception value of 0, with an assumed input impedance of 50 Ω, ensuring optimal operating conditions and antenna performance (Fig. 8c).

Directivity describes how an antenna radiates or receives RF energy in different directions. It can be expressed using a radiation pattern, which is a graphical representation of the field intensity as a function of azimuth and elevation angles.

The obtained azimuthal radiation patterns, both theoretical and measured, show that the proposed antenna radiates energy in a directionally dependent manner, meaning it is not omnidirectional. The antenna is designed to have a radiation pattern that is close to omnidirectional. These patterns represent a normalized power density distribution. Figure 9 represents the antenna's radiation patterns for selected frequencies. One may notice the measurement curves are identical to the calculated patterns.

4. Comparison with Other Designs

Table 2 presents a comparison of the parameters of the proposed design with other selected wide-band antennas from the literature in terms of impedance matching, profile (thickness),

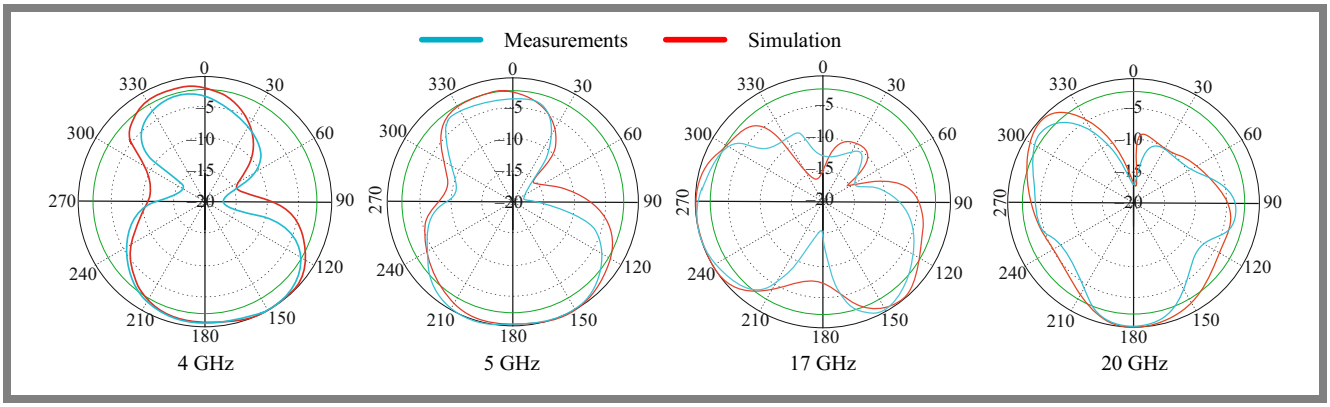


Fig. 9. Normalized directional characteristics in the azimuth plane.

and bandwidth. The operating bandwidth of the proposed antenna with respect to the S_{11} parameter is the highest compared to [3]–[8]. The calculated and measured values of the S_{11} parameter also show a high degree of convergence.

Based on the comparison of the electrical parameters of the proposed antenna with other designs, it was shown that the proposed broadband antenna exhibits comparable parameters in terms of matching impedance in all cases, especially in the case of stringent matching conditions [30].

5. Conclusions

The presented antenna is designed to operate in two frequency bands. Simulation results and measurements performed in an anechoic chamber (input impedance, reflection coefficient, and standing wave ratio) confirm its suitability for intended applications in radio communication systems. The wide operating bandwidth was achieved by using slots. Unfortunately, their size and location were determined through successive trials as part of an iterative design process. In further work, the authors plan to develop algorithms for automatic slot location planning according to the specified parameters.

References

[1] A.K. Arya, S.J. Kim, and S. Kim, "A Dual-band Antenna for LTE-R and 5G Lower Frequency Operations", *Progress In Electromagnetics Research Letters*, vol. 88, pp. 113–119, 2020 (https://doi.org/10.2528/PIERL19081502).

[2] I. Rodriguez *et al.*, "An Experimental Framework for 5G Wireless System Integration into Industry 4.0 Applications", *Energies*, vol. 14, art. no. 4444, 2021 (https://doi.org/10.3390/en14154444).

[3] W.E.I. Liu, Z.N. Chen, and X. Qing, "Metamaterial-based Low-profile Broadband Mushroom Antenna", *IEEE Transactions on Antennas and Propagation*, vol. 62, pp. 1165–1172, 2014 (https://doi.org/10.1109/TAP.2013.2293788).

[4] W.E.I. Liu, Z.N. Chen, and X. Qing, "Broadband Low-profile L-probe Fed Metasurface Wave Resonances", *IEEE Transactions on Antennas and Propagation*, vol. 68, pp. 1348–1355, 2020 (https://doi.org/10.1109/TAP.2019.2955629).

[5] W.Y. Sun and Y. Li, "Gain Stabilization Method for Wideband Slot-coupled Microstrip Antenna", *IEEE Transactions on Antennas and Propagation*, vol. 69, pp. 8932–8936, 2021 (https://doi.org/10.1109/TAP.2021.3097441).

[6] W. Liu, L. Zhu, W. Choi, and X. Zhang, "A Low-profile Differential-fed Patch Antenna with Bandwidth Enhancement and Sidelobe Reduction under Operation of TM and TE Modes", *IEEE Transactions on Antennas and Propagation*, vol. 66, pp. 4854–4859, 2018 (https://doi.org/10.1109/TAP.2018.2851393).

[7] W. Roh *et al.*, "Millimeter-wave Beamforming as an Enabling Technology for 5G Cellular Communications: Theoretical Feasibility and Prototype Results", *IEEE Communications Magazine*, vol. 52, pp. 106–113, 2014 (https://doi.org/10.1109/MCOM.2014.6736750).

[8] D. Wang, K.B. Ng, C.H. Chan, and H.Wong, "A Novel Wideband Differentially-fed Higher-order Mode Millimeter-wave Patch Antenna", *IEEE Transactions on Antennas and Propagation*, vol. 63, pp. 466–473, 2015 (https://doi.org/10.1109/TAP.2014.2378263).

[9] A. Gohar and G. Nencioni, "The Role of 5G Technologies in a Smart City: The Case for Intelligent Transportation System", *Sustainability*, vol. 13, art. no. 5188, 2021 (https://doi.org/10.3390/su13095188).

[10] A. Kakkar, Nirdosh, and S.A. Sah, "Multiband Circular Patch Microstrip Antenna for K and Ka Applications", *Intelligent Communication, Control and Devices, Advances in Intelligent Systems and Computing*, vol. 624, 2018 (https://doi.org/10.1007/978-981-10-5903-2_150).

[11] H. Ali *et al.*, "An Eight Element Dual Band Antenna for Future 5G Smartphones", *Electronics*, vol. 10, art. no. 3022, 2021 (https://doi.org/10.3390/electronics10233022).

[12] W. Liu *et al.*, "A Low-profile Differential-fed Patch Antenna with Bandwidth Enhancement and Sidelobe Reduction under Operation of TM and TM Modes", *IEEE Transactions on Antennas and Propagation*, vol. 66, pp. 4854–4859, 2018 (https://doi.org/10.1109/TAP.2018.2851393).

[13] D. Chaturvedi, B. Pramodini, and T. Lanka, "Compact MIMO Antenna with Extended Bandwidth Enabled by Parasitic Patch Structure", *Journal of Electromagnetic Waves and Applications*, vol. 39, pp. 1368–1379, 2025 (https://doi.org/10.1080/09205071.2025.2505051).

[14] M. Wnuk, "Two Methods to Analyze Microstrip Antennas for Wi-Fi Bandwidth", *Archives of Electrical Engineering*, vol. 70, pp. 705–719, 2021 (https://doi.org/10.24425/aee.2021.137583).

[15] Q.S. Liu, S. Sun, and W.C. Chew, "A Potential-based Integral Equation Method for Low-frequency Electromagnetic Problems", *IEEE Transactions on Antennas and Propagation*, vol. 66, pp. 1413–1426, 2018 (https://doi.org/10.1109/TAP.2018.2794388).

[16] S. Radavaram and M. Pour, "Wideband Radiation Reconfigurable Microstrip Patch Antenna Loaded with Two Inverted U-slots", *IEEE Transactions on Antennas and Propagation*, vol. 67, pp. 1501–1505, 2019 (https://doi.org/10.1109/TAP.2018.2885433).

[17] M. Wnuk, "Multilayer Dielectric Periodic Antenna Structure in a Cascade View", *Applied Sciences*, vol. 12, art. no. 4185, 2022 (https://doi.org/10.3390/app12094185).

[18] J. Park *et al.*, "Concept of Integrating 4G LTE and Millimeter-Wave 5G Antennas within Zero-bezel Cellular Devices", *2020 IEEE In-*

ternational Symposium on Antennas and Propagation and North American Radio Science Meeting, Montreal, Canada, 2020 (https://doi.org/10.1109/IEEECONF35879.2020.9330129).

[19] Y. Zou and J. Pan, "Broadband and High-gain Antenna Based on Novel Frequency Selective Surfaces for 5G Application", *4th Advanced Information Technology, Electronic and Automation Control Conference (IAEAC)*, Chengdu, China, 2019 (https://doi.org/10.1109/IAEAC47372.2019.8997989).

[20] J. Colaco and R. Lohani, "Design and Implementation of Microstrip Patch Antenna for 5G Applications", 5th International Conference on Communication and Electronics Systems (ICCES), Coimbatore, India, pp. 682–685, 2020 (https://doi.org/10.1109/ICCES48766.2020.9137921).

[21] K.A. Fante and M.T. Gemeda, "Broadband Microstrip Patch Antenna at 28 GHz for 5G Wireless Applications", *International Journal of Electrical and Computer Engineering*, vol. 11, pp. 2238–2244, 2021 (https://doi.org/10.11591/ijece.v11i3.pp2238-2244).

[22] S. Punith, S.K. Praveenkumar, A.A. Jugale, and M.R. Ahmed, "A Novel Multiband Microstrip Patch Antenna for 5G Communications", *Procedia Computer Science*, vol. 171, pp. 2080–2086, 2020 (https://doi.org/10.1016/j.procs.2020.04.224).

[23] Y. Ghazaoui *et al.*, "Millimeter Wave Antenna with Enhanced Bandwidth for 5G Wireless Application", *Journal of Instrumentation*, vol. 15, art. no. T01003, 2020 (https://doi.org/10.1088/1748-0221/15/01/t01003).

[24] M. Alam, R.I. Tomal, A.A.M. Faudzi, and N.A.T. Yuso, "ANN-Enabled Gain Prediction and Optimization in Dual-band SIW Antenna Designs for 5G Networks", *Journal of Telecommunication and Information Technology*, vol. 103, pp. 69–78, 2026.

[25] M.M. Kamal *et al.*, "A Novel Hook-shaped Antenna Operating at 28 GHz for Future 5G mmWave Applications", *Electronics*, vol. 10, art. no. 673, 2021 (https://doi.org/10.3390/electronics10060673).

[26] M.T. Gemeda, K.A. Fante, H.L. Goshu, and A.L. Goshu, "Design and Analysis of a 28 GHz Microstrip Patch Antenna for 5G Communication Systems", *International Research Journal of Engineering and Technology*, vol. 8, pp. 881–886, 2021.

[27] M. Hussain *et al.*, "Design and Characterization of Compact Broadband Antenna and its MIMO Configuration for 28 GHz 5G Applications", *Electronics*, vol. 11, art. no. 523, 2022 (https://doi.org/10.3390/electronics11040523).

[28] A.S.A. Gaid, M.A.M. Ali, A. Saif, and W.A.M. Mohammed, "Design and Analysis of a Low Profile, High Gain Rectangular Microstrip Patch Antenna for 28 GHz Applications", *Cogent Engineering*, vol. 11, art. no. 2322827, 2024 (https://doi.org/10.1080/23311916.2024.2322827).

[29] C.A. Balanis, *Antenna Theory: Analysis and Design*, 4th ed., John Wiley & Sons, Newark, 2016 (ISBN: 9781118642061).

[30] Y. Zhou and Y. Zheng, "A High-gain and Dual-band Compact Metasurface Antenna for Wi-Fi/WLAN Applications", *Materials*, vol. 18, art. no. 2538, 2025 (https://doi.org/10.3390/ma18112538).

Patrycja Okołot, M.Sc.
Department of Electronics
https://orcid.org/0009-0009-9536-0036
E-mail: patrycjaokolot@wp.pl
Military University of Technology, Warsaw, Poland
https://www.wojsko-polskie.pl/wat

Marian Wnuk, Professor
Department of Electronics
https://orcid.org/0000-0003-4576-4023
E-mail: marian.wnuk@wat.edu.pl
Military University of Technology, Warsaw, Poland
https://www.wojsko-polskie.pl/wat

Konrad Szczepankiewicz, M.Sc.
Department of Electronics
https://orcid.org/0000-0003-3292-8113
E-mail: konrad.szczepankiewicz@wat.edu.pl
Military University of Technology, Warsaw, Poland
https://www.wojsko-polskie.pl/wat